Applications of H/C Surface Chemistry to wall materials in fussion devices and low pressure diamond synthesis

S. Ishi

Tomakomai National College of Technology,
Tomakomai, 059-12

J.Biener, C.Lutterloh, J.Küppers*
Experimentalphysik VI, Universität Bayreuth,
Bayreuth 95440, Germany
(Received 18 November. 1996)

Abstract

The present review shows recent works of structures and reactions of thin C:H films with and without thermal hydrogen atoms exposed by High Resolution Electron Energy Loss Spectroscopy and Thermal Desorption Spectroscopy. Reaction mechanisms of hydrogenation and dehydrogenation at C:H films under thermal H exposed reveal the erosion reaction of C:H films.

1 Introduction

Investigations of structures and properties of H-terminated surfaces have been interested from both a technological and scientific point of view[1]. The present article focusses on the elucidation of structures and elementary steps of reactions at C:H films, the system of which is considered to be the model ones of the interaction of plasma with carbon-wall in fussion devices and low pressure diamond synthesis. Studies of structures and reactions at C:H films with Electron Energy Loss Spectroscopy (HREELS) and Thermal Desorption Spectroscopy (TDS) are presented. It is seen that these basic studies are closely connected with the understanding of wall materials in fussion devices and low pressure diamond synthesis.

The contents in the present review are as follows. The section 2 describes the preparation and some properties of ultra thin C:H films. The sections 3 and 4 show and illustrate spectra of vibrational structures and thermal decompositions of C:H films, respectively. The section 5 shows reaction mechanisms of hydrogenation and dehydrogenation at C:H films by thermal H exposed. These elementary steps of reactions compose the cycle of erosion reaction at C:H films. The final section discusses the doping effect of boron in C:H films.

2 Preparation of C:H films[2]

C:H films, which is considered to be a model system for low pressure diamond synthesis and wall materials in fussion devices, is prepared on graphite monolayer covered Pt single crystal surfaces in a UHV environment. The graphite monolayer is deposited, for example, by thermal decomposition of ethylene at 730 K. A role of the graphite monolayer, which is crystallized, may serve as a carrier for deposition of C:H films only. The graphite monolayer covered Pt single crystal surfaces is represented as the substrate in what follows.

The deposition of C:H filmes is performed by an ion-beam-deposition of the so-called process or feed gas, which is hydrocarbon, for example, CH_4, C_2H_2, C_2H_4 and so on. The amount or thickness of C:H films, which is not crystallized, was determined with Auger spectra by

* Max-Planck-Institut für Plasmaphysik (EURATOM Association), Garching 85748, Germany

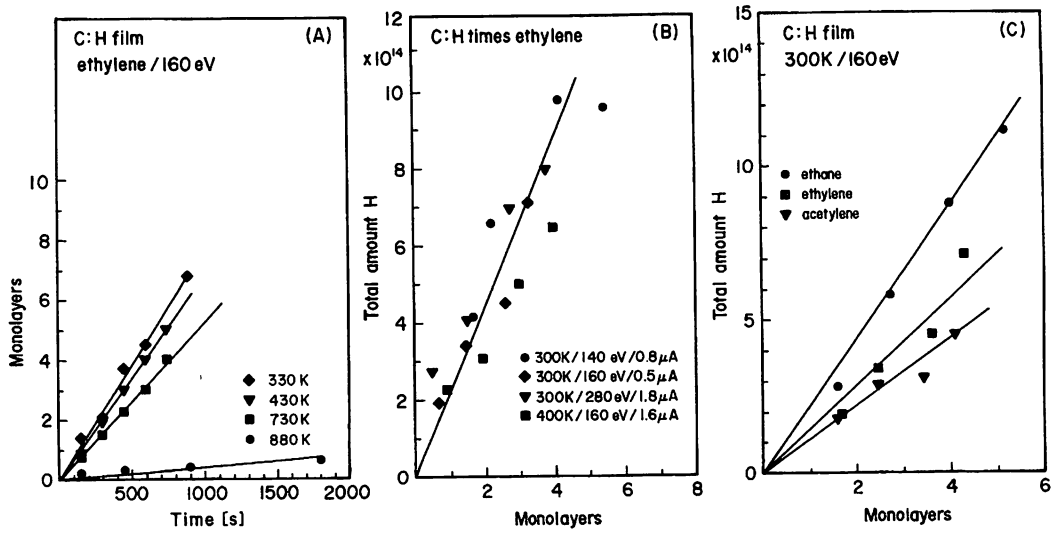

Fig.1 (A) Thickness of C:H films as a function of deposition time (process gas: ethylene, ion energy: 160 eV).
(B) Amount of H released from C:H films grown from ethylene at different temperatures, ion energies, and target currents.
(C) Amount of H released upon thermal decomposition of C:H films grown from different process gas with various thickness.

using the C monolayer signal for calibration and is represented in unit of monolayer, ML. One monolayer, 1 ML is equal to the atom density of the graphite (0001) surface, i.e., 1 ML=3.8 $*10^{15}cm^{-2}$.

The hydrogen content on C:H films was measured by heating the films from 300 K to 1400 K, which is sufficient for other thermal decomposition. Simultaneously, the signals of hydrocarbons of C_1- and C_2-species were monitered.

The formation of C:H films is dependent on hydrocarbon species and their ion energies, target currents and substrate temperature. The experimental results about thickness of C:H films as a function of deposition time on substrate temperatures (330 K (◆), 430 K (▼), 730 K (■), and 880 K (●)) are shown in Fig.1 (A). It is seen that the gradients at fixed temperature linearly increase with respect to deposition time. It should be noted that the gradient at 880 K substrate temperature is particularly small in comparison with other gradients. This is due to the chemical erosion reaction as may explain later.

Fig.1-(B) and -(C) at C:H films grown from ethylene, where we consider the deposition conditions, substrate temperatures, ion energies and target currents, show the amount of H released from C:H films as a function of thickness (monolayer). It is seen from Fig.1-(B) that for a fixed process gas, ethylene, the H content of the films grows linearly in a narrow temperature and ion energy range. However, the actual amount of hydrogen in the films is affected by the number of H atoms which carried by the process gas molecule. Fig.1-(C), where C:H films to be observed have grown from different process gases, C_2H_6(●), C_2H_4(■) and C_2H_2(▼), suggests that the deposition of hydrogen-richer species causes the H content of the films to increase. The effective range of ion energies for deposition is found to be 160 - 300 eV.

According to a result, which we shall show in the next section (see Fig.2 (D)), we can state that the vibrational structures of C:H films grown from these process gases are very similar.

As an example, we shall take a C:H films, which is deposited from 160 eV ethane ions at 350 K substrate temperature. Then, the [H]:[C] ratio is about 0.4 - 0.5, where the bracket [A] denotes the concentration of A species anyway.

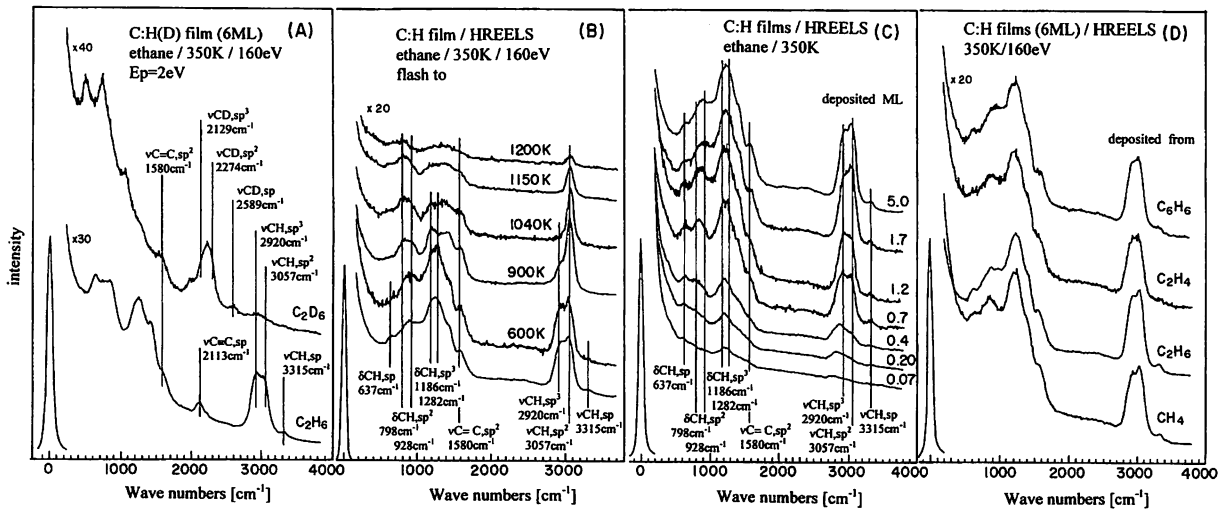

Fig.2 HREEL spectra at 6 monolayers of C:H or C:D films under various conditions:
(A) spectra ion-beam deposited from ethane and fully deuterated ethane at 350 K substrate temperature.
(B) spectra with increasing temperature.
(C) spectra with different thickness.
(D) spectra deposited from various hydrocarbons.

These films have a similar structure of μm thick a-C:H films deposited by plasma assisted chemical deposition (PACVD).

3 Vibrational properties of C:H films[3-5)]

In this and following sections we shall show several spectra with high-resolution electron energy spectroscopy (HREELS), which is powerful to identify surface species.

HREEL spectra of six monolayers thick C:H and C:D films deposited from ethane at 160 eV ion energy and 350 K substrate temperature are shown in Fig.2 (A), where typical assignments of C—H(D) and C—C modes are determined on the basis of those of gaseous hydrocarbons and isotope effect:

Frequencies(cm^{-1})	Assignments
3315 and 2113	νCH (sp) and ν C≡C
3057 and 1580	νCH (sp^2) and aromaticC=C
2990	νCH_m (sp^3) m=1,2,3

C—H bonds in C:H films are characterized by the terms of hybridization states of C atoms, which are specified as sp, sp^2, and sp^3. νCH(sp), ν CH (sp^2), and ν CH (sp^3) mean the stretch vibration of C—H bond with sp, sp^2, and sp^3 hybridization states of C atom, respectively. It should be noted that alkene-type sp^2 hybridized CH_2 bond is absent and that alkane-type sp^3 hybridized C—H bond has the possibility of CH_m (m=1,2,3). νC≡C and aromaticC=C denote the stretch mode of linear C—C triple bond and aromatic ring mode of C—C double bond, respectively. Here we comment that the spectra in Fig.2 (A) shows the close resemblance to IR spectra taken at μm thick a-C:H films deposited by PACVD[6)] and HREEL spectra at thin polyethylene films[7)].

The ratio of [sp^2]:[sp^3] in C:H films is found to be nearly unity by measurements of electron energy loss of plasmon and its related analysis. The amount of [sp] is a minor one[5)].

HREEL spectra of C:H films with various substrate temperatures are shown in Fig.2 (B). Typical changes of various modes of adsorbates to increasing temperature are:

1. νCH(sp) mode disappears above 600 K.
2. νCH_m(sp^3) mode disappears above 1040 K.
3. νCH(sp^2) mode is seen up to 1200 K.

These results show that the ordering of the stability of ν CH with various C-hybridization states for increasing temperature is sp < sp^3 <

sp^2. The unstability of ν CH(sp) is due to the high reactivity of the alkyne type sp hybridization as well-known in organic chemistry.

HREEL spectra of C:H films various film-thickness are shown in Fig.2 (C). The spectra with more than 0.7 ML are resemble to those in Fig.2 (A). This shows that the structure of C:H films is similar irrespective of film-thickness except submonolayer, which is less than 0.7 ML. At ML $\rightarrow$ 0, ν CH (sp^3) seems to be dominant. Then, upon submonolayer the substrate certainly influences adsorbates. But, do not worry about it because we do not deal with a submonolayer in the context.

Finally, we shall show Fig.2 (D) as mentioned at the end in the previous section, where HREEL spectra from various species of hydrocarbons CH_4, C_2H_2, C_2H_4 and C_2H_6 at 350 K substrate temperature are taken. All spectra are very similar irrespective of different species. As a different point, the [H]:[C] ratios of C:H films changes from 4 : 1 to 1 : 1 according to increase of the number of H atoms in hydrocarbon.

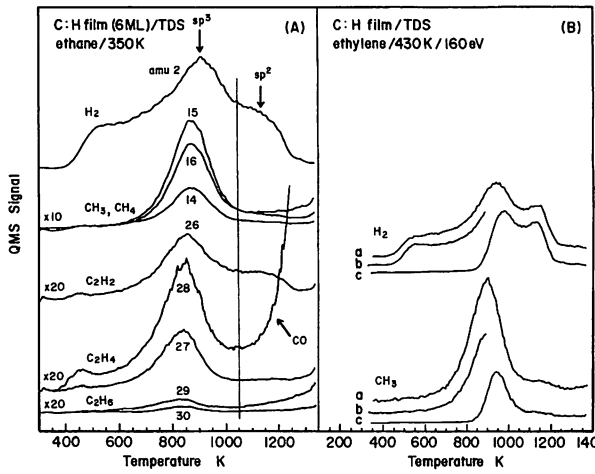

Fig.3 (A) TD spectra of hydrogen, methane and various hydrocarbons during thermal decomposition of 6 monolayers C:H films from ethane at 350 K. Heating rate 5 K/s. (B) TD spectra of hydrogen and methyl radical at recpective 6 monolayers C:H films from ethylene at 350 K. (a) full spectra as in Fig.3 (A). (b) spectra with interrupped ramp at 900 K. (c) full spectra subsequent to taking data for set (b).

4 Thermal decomposition of C:H films[2,4)]

Thermal desorption spectra from C:H films as prepared in Fig.2 (A) are shown in Fig.3 (A). It should be noted that the desorption of H_2 below 600 K is due to H atoms adsorbed from the substrate, not to be due to the C:H films of consideration. In desorption species, molecular hydrogen is a dominant component, 90% while hydrocarbons minor ones. The components and their related temperatures of desorption spectra are summarized as follows:

species	T range [K]	T max [K]	contribution[%]
H_2	600 to 1200	920	90
CH_3	700 to 1000	880	2
CH_4	700 to 1000	880	4
C_2H_2	700 to 1250	850,1150	1
C_2H_4	700 to 1000	850	2
C_2H_6	700 to 1000	850	<1
C_nH_m ($n \geq 3$)	700 to 1250	850,1150	<1

Most notable is the fact in Fig.3 (A) that the temperature dependence of the desorption rates of methyl and methane are identical, apart from a scaling foctor.

Fig.3 (B) shows desorption spectra of hydrogen molecule and methyl radical, where the traces (a), (b) and (c) correspond to the following procedures:

(a) full spectra to increasing temperature from 350 K to 1400 K
(b) spectra with interrupted ramp at 900 K
(c) full spectra subsequent to taking data for the set (b)

This result shows that hydrogen and methyl in different chemical environment are released at different temperatures. The same holds for other species observed upon thermal decomposition of the C:H films as seen in Fig.3 (A) and the above table. The apparent desorption order of the gas release may be unity as a decrease of the respective species concentrations has no influence on the desorption temperature range.

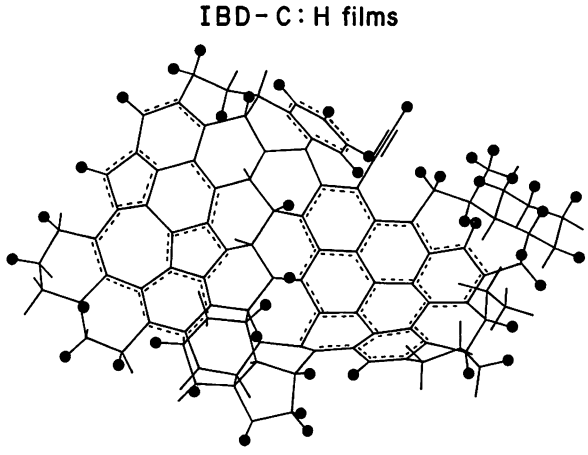

Fig.4 A model of $C_{network}$

From these, we shall consider the desorption mechanisms and rates of CH_3, CH_4 and H_2. At first, the desorption mechanisms of methyl radical and methane may be represented as

$$C_{network}\text{-}CH_m(sp^3) \rightarrow C_{network} + CH_3\uparrow$$

and

$$C_{network}\text{-}CH_m(sp^3) \rightarrow C_{network} + CH_3 + H \rightarrow C_{network} + CH_4\uparrow$$

where we do not distinguish the insignificant difference of $C_{network}$ between the first and other columns. The illustration of $C_{network}$ is given in Fig.4[4].

The rate equation of desorption for CH_3 is analysed as the following first order of desorption

$$-\frac{d[CH_3]}{dt} = [-CH_m(sp^3)]\,\nu \exp\left(-\frac{E_{ac}}{kT}\right) \quad (1)$$

assuming that $\nu = 10^{13}(s^{-1})$ and $E_{ac} = 57\left(\frac{Kcal}{mol}\right)$. The range of desorption temperature is about from 700 K to 1000 K while that estimated by the above equation about from 700 to 900 K. This difference between experiment and theory refers to the heterogeneity of C:H films surfaces. Thus, we may assume that activation energies exhibit a $10\left(\frac{Kcal}{mol}\right)$ wide Gaussian distribution at $57\left(\frac{Kcal}{mol}\right)$, that is, $E_{ac} = 57 \pm 10\left(\frac{Kcal}{mol}\right)$. The comparison between experimental and theoretical desorption traces is shown in Fig.5, where two calculated desorption curves of first order with Gaussian distributed activation energies of widths zero and $10\left(\frac{Kcal}{mol}\right)$ around 56

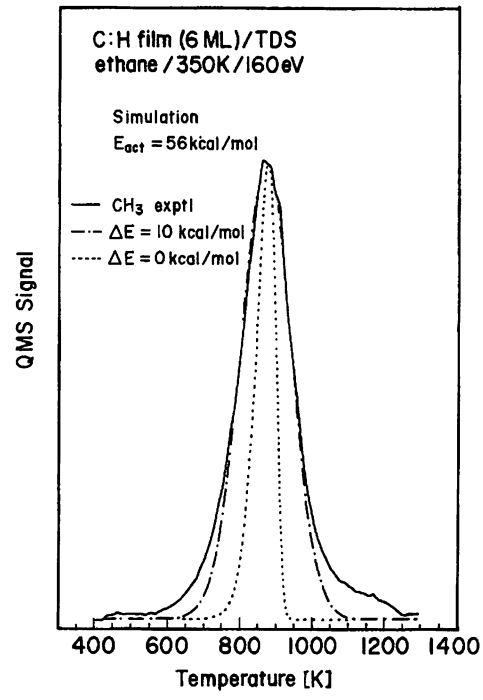

Fig.5 Comparison between calculated and experimental desorptions of methyl. The broken and the dotted-broken curves are with and without assuming a distribution of activation energies, respectively.

$\left(\frac{Kcal}{mol}\right)$ are shown by broken and broken-dotted curves, respectively.

The rate equation of desorption for CH_4 may be similar to that for CH_3. It is because CH_3 bond breaking in $C_{network}\text{-}CH_m(sp^3)$ is rate determining, namely, during desorption of CH_4 the concentration [H] is nearly constant as compared with the concentration $[CH_3]$.

The desorption of molecular hydrogen has a maximum peak at 920 K and a shoulder at around 1120 K. These temperatures closely correlate the temperature dependence of HREEL spectra in Fig.2 (C), namely, above 900 K the peak of sp^3 is not seen and above 1040 K that of sp^2 is only seen. Then, the desorption mechanism of H_2 may be represented as

$$H_mC\text{-}C_{network}\text{-}CH_m(sp^3) \rightarrow C_{network} + H + H \rightarrow C_{network} + H_2\uparrow$$

and

$$H_mC\text{-}C_{network}\text{-}CH_m(sp^2) \rightarrow C_{network} + H + H \rightarrow C_{network} + H_2\uparrow$$

In lower temperature the former scheme is predominant while in higher temperature the latter scheme only occurs. The rate equation of H_2 desorption may be written

$$\frac{d[H_2]}{dt} = \nu[H]^2 \exp\left(-\frac{E_{ac}}{kT}\right)$$
$$\simeq \sum_{i=2}^{3} \nu'[CH(sp^i)]\exp\left(-\frac{E_{ac}(sp^i)}{kT}\right) \quad (2)$$

as $CH(sp^i)$ bond breakings from $C_{network}$ are rate determining. About the rate equation (2) it is assumed that ν' is taken to be $10^{13}(s^{-1})$ and $E_{ac}(sp^i)$ Gaussian distributed around 59 and 69 $\left(\frac{Kcal}{mol}\right)$ with $\pm 3\left(\frac{Kcal}{mol}\right)$. The argument concerning the effect of heterogeneity on the activation energy for CH_3 and CH_4 also applies. The above study can be used to understand the elementary steps of the much debated phenomenon of hydrogen-induced erosion reaction of carbon based wall materials in fussion related plasma experiments.

5 Reactions of C:H films at H(D) exposed

5.1 Hydrogenation of C:H films under thermal H(D) atoms[8)]

Thermal H (D) atoms were generated by dissociation in a resistively heated tantalum tube (1900 K) with a small effusion orifice (0.1 mm) at an inner tube pressure of 10^{-2} Torr H_2 (D_2) and its flux is estimated to be about $8.5 \cdot 10^{11}$atoms($s^{-1}cm^{-2}$).

HREEL spectra are shown in Fig.6 (A), where the C:H films surfaces were exposed at 350 K substrate temperature to a fluence of 0.4 ML D (H) atoms. It is obviously seen from the different spectrum (b)-(a) that the intensity of sp^2 species decreases and that of sp^3 increases due to the influnce of D (H). Then, this process of hydrogenation is schematically written

$C_{network}$-CH(sp) + thermal H → $C_{network}$-$CH_{2,3}(sp^3)$
or
$C_{network}$-H(sp^2) + thermal H→ $C_{network}$-$CH_{2,3}(sp^3)$

To confirm the hydrogenation of sp^2 to sp^3 further, such C:H films, which is flashed to 1040 K and then is cooled down to 350 K, is prepared. By the use of such C:H films, after exposed to an increasing flux of thermal D atoms at 350 K HREEL spectra are taken. The spectra obtained with various H exposures are shown in Fig.6 (B), where the intensity of sp^3 increases with respect to increasing H exposure as expected.

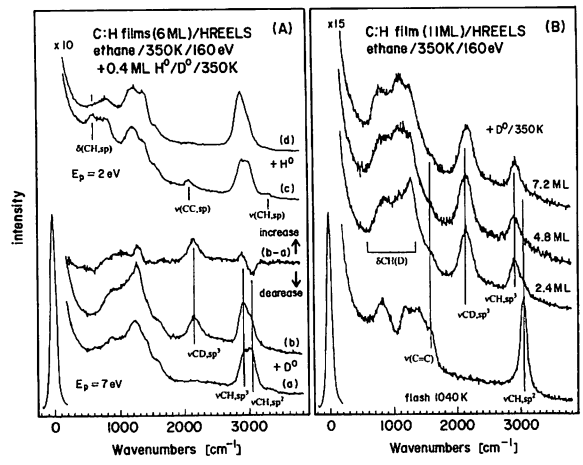

Fig.6 (A) HREEL spectra at C:D films (a,b) and C:H films (d,e) of 6 monolayers thickness with a fluence 0.4 ML of thermal hydrogen. Dosing time 1800 s. (B) HREEL spectra at 11 monolayers C:H films with various thermal D exposures. The bottom spectrum flashed to 1040 K and cooled down to 350 K.

The rate equation of hydrogenation from sp^2 to sp^3 may be represented

$$-\frac{d[sp^3]}{dt} = [sp^3]\sigma_H \Phi \quad (3)$$

where σ_H is the hydrogenation cross section and Φ a flux of thermal H atoms as given above. The cross section of hydrogenation is estimated to be about 4.5 $Å^2$.

These experimental results demonstrate the proposition of Deryaguin et at[9)]. that atomic hydrogen plays a key role in the low pressure diamond synthesis via removal of the graphite co-deposit.

5.2 Dehydrogenation of C:H films under thermal H(D) atoms[10)]

As described above, C:H films has completely hydrogenated by a fluence of more than 7 ML of H atoms (see Fig.6 (B)). HREEL spectra after exposing the hydrogenated surfaces to a

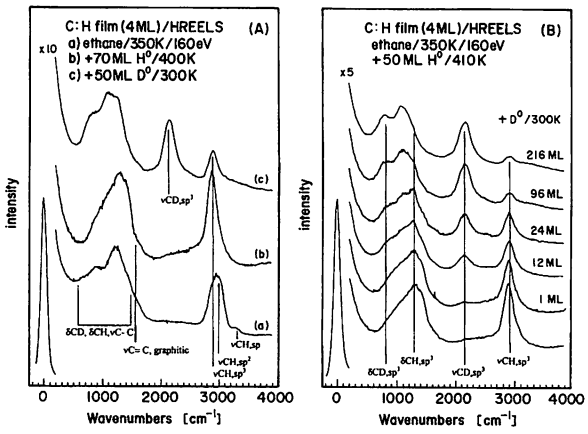

Fig.7 HREEL spectra under various conditions: (a) spectra at C:H films ~4 monolayers as in Fig. 3 (A). (b) spectra after full hydrogenation with a 70 ML dose of H atoms. (c) spectra after exposing the hydrogenated surface to a 50 ML dose of D atoms (B) HREEL spectra at ~4 monolayers C:H films with various D exposures. D atoms were exposed at 300 K.

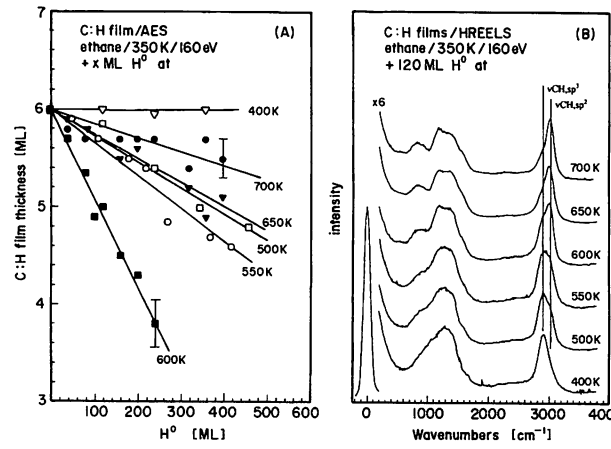

Fig.8 Thickness of an initially 6 monolayers ion-beam deposited C:H films as a function of H atom fluence at various temperatures. (B) HREEL spectra measured exposing 6 monolayers C:H films to a 120 ML of thermal H atoms at various temperatures.

50 ML dosed of D atoms are shown in Fig.7 (A). It is seen from the spectrum (c) that the surface of (b) are dehydrogenated by D atoms on the basis of a well-grounded finger-print for ν CH sp^3. This dehydrogenation scheme may be written

$$C_{network}\text{-}CH_m\ (sp^3) + \text{thermal D} \rightarrow C_{network}\text{-}C^*H_{m-1} + HD\uparrow$$

where * means the radical of C atom. Instead of the term dehydrogenation, it may say that this process is the hydrogen abstraction by thermal deuterium atoms. Simultaneously, the following scheme of hyrdogenation proceeds

$$C_{network}\text{-}C^*H_{m-1}\ (sp^2) + \text{thermal D} \rightarrow C_{network}\text{-}CH_{m-1}D$$

The reaction of hydrogenation, the latter reaction scheme proceeds faster than the reaction of dehydrogenation, the former scheme as well known.

Fig.7 (B) shows HREEL spectra with various D exposures, where the C—D (sp^3) stretch vibrational intensity increases with respect to increase of D exposure. By assuming that this C — H stretch loss peak intensity, I [C-H] can serve as a measure of H concentration, the rate equation of dehydrogenation is expected by

$$-\frac{d[sp^3]}{dt} = [sp^3]\sigma_D \Phi \qquad (4)$$

where σ_D is dehydrogenation cross section. The cross section of dehydrogenation is estimated to be about 0.05 $Å^2$.

This study of the hydrogen abstraction by hydrogen atoms is the first directly instrumental identification in low diamond synthesis and related processes.

5.3 Chemical erosion of C:H films under thermal H atoms[11)]

The film thickness of initially six monolayer thick C:H films as a function of H atom fluence and film temperature during H exposure is shown in Fig.8 (A), where the linear decrease at 600 K is notable in comparison with those at lower and higher temperatures with respect to 600 K.

HREEL spectra observed after exposing 6 monolayer thich C:H films to 120 ML of thermal H atom at various temperatures are shown in Fig.8 (B), where the peak intensity of ν CH(sp^2) increases and one of ν CH(sp^3) decreases to increasing temperature, from 400 K to 700 K.

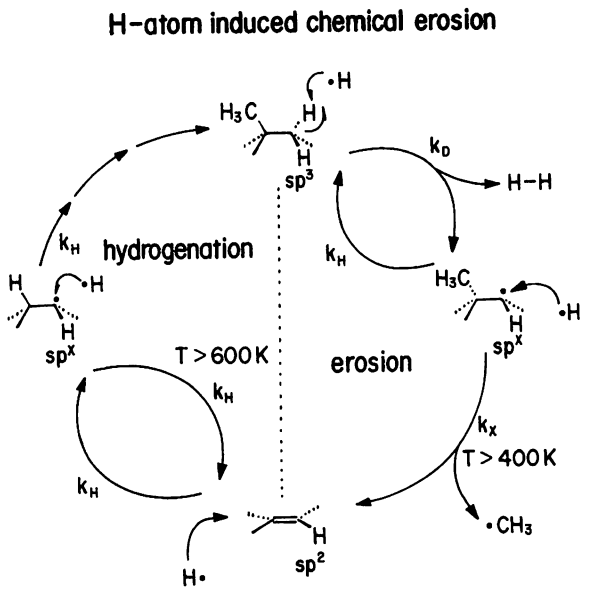

Fig.9 Scheme of erosion reaction at C:H films.

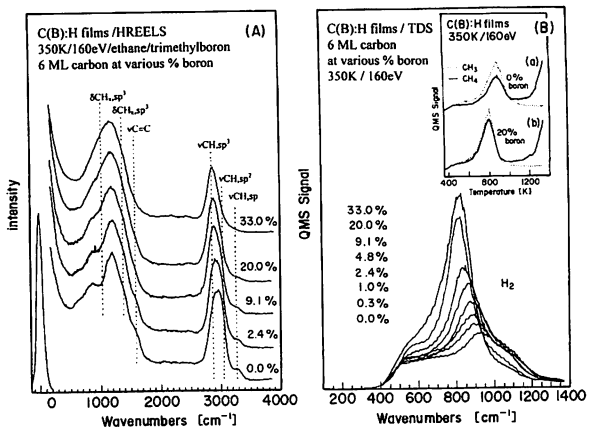

Fig.10 (A) HREEL spectra at C:H films with various boron contents. (B) TD spectra of hydrogen molecule ; TD spectra (a) and (b) of methyl and methane with and without boron in inset.

From these results, it is suggested that this change is correlated with the erosion reaction under thermal H atoms, which is equivatently described as the H impact induced erosion reaction. Therefore, the temperature about 600 K in Fig.8 (A) means to be a most effective one for the H impact induced erosion reaction. Then, together with hydrogenative and dehydrogenative reactions as described above, the following reaction scheme may be written

$$H_3C\text{-}C_{network}\text{-}C^*H_x + \text{thermal H} \rightarrow C_{network} + CH_3\uparrow$$

where the activation energy of erosion is estimated to be about 40 $\left(\frac{\text{Kcal}}{\text{mol}}\right)$. This erosion reaction competes between the supply of C^* radicals and temperature. The erosion efficiency drops towards lower and higher temperature as seen in Fig.8 (A). The decrease towards lower temperature is caused by the activation energy for erosion reaction, while the decrease towards higher temperature by the lock of the supply of C^*. This maximum temperature at about 600 K for H-induced erosion reaction is lower than that at 880 K for the thermally excited erosion one in the previous section.

By summarizing various reaction steps described above, we shall show Fig.9 about the scheme of reactions which are initiated by H impact and temperature at C:H films or other hydrogenated carbon substrates. On the left of Fig.9 the reaction sequence of hydrogenation of a sp^2 entity via an intermediate radical 'sp^x' state is shown. This cadical intermediate is necessary as one H atom can only hydrogenate one C center at a time. Therefore, the neighboring C center must assume this sp^x state. Repetitive application of hydrogenation with a final C—C bond-breaking which may involve rearrangements will lead to, for example, a methyl group as indicated in the figure. On the right of Fig.9 the H atom impact induced dehydrogenation reaction of a sp^3 entity via molecular hydrogen release is drawn. Clearly, this reaction also has an intermediate radical sp^x product. This radical intermediate may saturate to sp^3 through hydrogenation.

This investigation of elementary steps about chemical erosion reaction in C:H films may debate to make those in low pressure diamond synthesis clear.

6 C:H films by boron doping[12)]

In order to investigate the effect of boron doping into C:H films, the films were prepared by operating an ion gun in a feed gas which contained mixtures of ethane/trimethyleboron (TMB) and were deposited at 160 eV ion energy and 350 K substrate temperature as discribed

above.

HREEL spectra with various boron contents (0.0% – 33%) are shown in Fig.10 (A), where the νCH_m (sp^3) peak intensity is dominant as B content increases. This result necessarily leads to the increase of H content. The ν BH mode is not seen in the spectra although it may be very remarkable.

Thermal desorption spectra of H_2 (a), CH_3 and CH_4 (b) are shown in Fig.10 (B). It is seen that the peak maximums of each species shift to lower temperature by comparison of these of undosed C:H films. This result only identifies that the activation energy of desorption for B—CH_m (sp^3) is smaller than that for C—CH_m (sp^3). The efficiency of chemical erosion relatively decreases due to high content of B atoms. It should be noted that a shoulder at around 1120 K at undoped C:H films for H_2 desorption disappears with increasing Boron content.

These experimental results comfirm that the microscopic pictures of the boron doping effect deduced from the model systems apply for the bulk samples such as wall materials in fussion devices.

References

1) For example, J.Küppers, Surf. Sci. Reports, Vol 22,Nos 7/8, 249-322 (1995)

2) A.Schenk, B.Winter, J.Biener, C.Lutterloh, U.A.Schubert and J.Küppers, J. Appl. Phys. 77 (6), 2462 (1995)

3) J.Biener, A.Schenk, B.Winter and J.Küppers, J. Electron Spectro. and Related Pheno. 64/65, 331 (1993)

4) J.Biener, U.A.Schubert, A.Schenk, B.Winter, C.Lutterloh and J.Küppers, J. Chem. Phys. 99 (4), 3125 (1993)

5) J.Biener, A.Schenk, B.Winter, U.A.Schubert, C.Lutterloh and J.Küppers, Phys. Rev. B 49, 17307 (1994)

6) B.Dischler, A.Bubenzer and P.Koidl, Solid State Commum. 48, 105 (1983)

7) J.J.Pireaux, P.A.Thiry, R.Candano and P.Pfluger, J. Chem. Phys. 84, 6452 (1986)

8) J.Biener, A.Schenk, B.Winter, C.Lutterloh, U.A.Schubert and J.Küppers, Surf. Sci. 307-309, 228 (1994)

9) B.V.Deryagin, D.V.Fedeseev, V.M.Lukyanovich, B.V.Spitsyn, V.A.Ryabov and A.V.Lawrentyev, J. Cryst. Growth. 2, 380 (1969); B.V.Deryagin, L.L.Bouilov, B.V.Spitsyn, Arch. Nauki Mater. 7, 111 (1986)

10) C.Lutterloh, A.Schenk, J.Biener, B.Winter and J.Küppers, Surf. Sci. 316 (1994) L1039

11) A.Horn, A.Schenk, J.Biener, B.Winter, C.Lutterloh, M.Wittmann and J.Küppers, Chem. Phys. Lett. 231 (1994) 193

12) A.Schenk, B.Winter, C.Lutterloh, U.A.Schubert, J.Biener and J.Küppers, J. Nucl. Mater. 220-222, 767 (1995)